Importance of Mesoscale Eddies and Mean Circulation in Ventilation of the Southern Ocean

Igor Kamenkovich,

RSMAS, University of Miami, Miami, FL

Zulema Garraffo,

IMSG at NOAA/EMC, College Park, MD

Romain Pennel,

LMD, Ecole Polytechnique, Palaiseau, France

Rana A. Fine,

RSMAS, University of Miami, Miami, FL

Abstract

This study examines the relative importance of the mean advection and mesoscale currents in the property exchange between the Southern Ocean mixed layer and downstream in the upper 2000 meters; this exchange is referred to as ventilation. A new, highly efficient offline tracer model employed here uses pre-calculated velocities to advect dynamically passive tracers. Two idealized tracers are considered: the Boundary Impulse Response (BIR) tracer, which helps to determine the ventilation pathways and time scales, and the Transient Surface Tracer (TST), which is relevant to transient atmospheric tracers. The importance of eddies is isolated by contrasting the control simulation with a simulation without mesoscale currents. The analysis reveals complex three-dimensional ventilation pathways, controlled by the interplay between the mean advection and eddy-induced spreading. The mean currents carry the tracers eastward within ACC and contribute to the formation of the Antarctic Intermediate Water (AAIW) in the South Pacific and South Atlantic. The main effect of eddies is to disperse tracers away from the mean pathways, and this dispersion acts to retain the BIR tracer in the Atlantic and Indian sectors and reduce the upstream influence of these regions on the South Pacific. In addition, the eddy-induced along-isopycnal spreading within ACC increases the ventilated depth and the inventory of TST. The results can be used to interpret distribution of tracers in the ocean in numerical simulations and observations.

1 Introduction

The Southern Ocean south of 30°S accounts for a disproportionately large share of the exchange of properties between the atmosphere, surface waters and the deep ocean. Despite occupying just over one third of the surface ocean area, the Southern Ocean may account for up to half of the annual oceanic uptake of anthropogenic carbon dioxide from the atmosphere (*Gruber et al.,* 2009) and for about 70 ± 30% of the excess heat that is transferred from the atmosphere into the ocean each year (*Frölicher et al*. 2015). This study aims to establish the relative importance of advection by mesoscale eddies and mean currents in the transfer of properties from the Southern Ocean mixed layer into the deep oceanic interior, and in determining the associated pathways and timescales.

Ventilation is defined here as the process by which water, tracers and gases are transferred from the surface mixed layer into the upper 2000 meters of the oceanic interior. In the upper ocean, vertical turbulent mixing contributes to formation of the deep mixed layer and Subantarctic Mode Water (SAMW; *McCartney* 1977; *Sloyan et al.* 2010); these processes facilitate uptake of heat and atmospheric gases. These uptakes are modulated by the presence of mesoscale eddies in the region (*Sallee et al.* 2012; *Song et al.* 2015). Additional processes include convection and downslope flows, which lead to the formation of the very dense Antarctic Bottom Water (AABW). Below the mixed layer, the role of diapycnal exchange diminishes away from the topography, and adiabatic, along-isopycnal advection becomes an important process in tracer distributions. Most notably, along-isopycnal subduction plays a key role in the formation of the Antarctic Intermediate Water (AAIW) which originates in the deep pycnostad associated with

SAMW and ventilates the subtropical gyres (*McCartney* 1977; 1982). AAIW formation sites are located near the South American continent in the South Pacific (*Reid* 1965) and in the confluence of the Malvinas and Brazil Currents in the Atlantic basins (*Talley* 1996); a significant portion of AAIW also enters the Atlantic through the Drake Passage (*Sloyan and Rintoul* 2001). AAIW is characterized by distinct salinity minimum (salinities 32.2-32.4 ppt, densities $\sigma_\theta = 27.0 – 27.4$ kg m^{-3}; e.g. *Talley* 1996) and oxygen maximum at the formation latitudes; although these extrema are diluted further downstream by exchanges with surrounding waters, still AAIW can be traced into the Northern Hemisphere (e.g. *Reid* 1965; *Tsuchiya* 1991).

Along-isopycnal advection can be separated into a large-scale mean component, which includes the Antarctic Circumpolar Current (ACC) and western boundary currents of the subtropical gyres, and mesoscale eddies. Mesoscale eddies, defined here as deviations from the mean flow, are widely believed to play an important role in the Southern Ocean dynamics and tracer distributions. This importance represents a major challenge for climate models, which are unable to afford high spatial resolution required for accurate simulation of these motions in the ocean, especially at high latitudes. Instead, numerical models can (at best) only partially resolve the mesoscale and often have to rely on eddy parameterizations. Assessment of the role of eddies in ventilation of the Southern Ocean can, therefore, help to evaluate and improve these models by identifying specific regions and processes in which eddy-induced stirring is important.

Analysis of the relative importance of the mean and eddy advection is, however, challenging, because their effects on tracer distribution are closely intertwined. The mean state is in large part determined by eddies (e.g. *Marshall and Radko* 2003), and a numerical simulation with large biases in eddy dynamics will have an incorrect mean state as well. Progress in this direction can

75 be achieved by focusing on the direct kinematic effects of eddies. One particularly effective
76 method is to contrast distributions of dynamically passive tracers in two simulations with identi-
77 cal mean circulation, but with and without eddies (*Booth and Kamenkovich* 2008). This approach
78 is taken in this study that employs an offline tracer model which uses pre-calculated mass fluxes
79 to advect idealized passive tracers. The advantages of this method are two-fold. First, such of-
80 fline model has very high computational efficiency that enables multiple extended calculations.
81 Second, the offline formulation permits studies of the sensitivity of transport properties of the
82 flow to the presence of various components of the velocity field (e.g., mesoscale eddies), and this
83 property is essential for this study. In addition, the offline formulation permits an explicit evalua-
84 tion of eddy parameterization schemes, but such evaluation is not attempted in this study.

85 The ventilation efficiency and pathways, and a response to surface boundary forcing in gen-
86 eral, can be conveniently examined using idealized tracers. Quantification of the time-dependent
87 response to surface boundary forcing requires knowledge of the dependence on the *transit time*,
88 or time that has passed since a particular surface forcing event. In the presence of an unsteady
89 flow and/or sub-grid mixing, the response will also depend on the time of the forcing event, and
90 can be quantified by the boundary impulse response (BIR) function. Alternatively, the distribu-
91 tion of the time-dependent responses with transit times is called "transit time distribution"
92 (TTD); TTD and BIR are equivalent for a steady flow. BIR is calculated from a response to an
93 instant impulse of a surface tracer at a given time and infinitely small surface area (*Holzer and*
94 *Hall* 2000; *Khatiwala et al.* 2001; *Haine and Hall* 2002). An arbitrary tracer can be derived from
95 its distribution at the surface and BIR. Because of obvious numerical limitations, however, both
96 the duration of the impulse and the source region area are made finite (*e.g. Khatiwala et al.* 2001;
97 *Haine and Hall* 2002; *Peacock and Maltrud* 2006). An ensemble of BIRs, integrated for very

long time, can be used to derive an "ideal age" of water masses (*Hall and Haine* 2002; *Haine et al.* 2008; *Maltrud et al.* 2010), which is the average time since the water was last directly exposed to the atmosphere (*Thiele and Sarmiento* 1990; *England* 1995).

In this study, propagation of a single BIR pulse from the ocean mixed layer into ocean interior provides valuable information on the ventilation pathways and timescales. A second idealized tracer considered here mimics evolution of a transient atmospheric tracer, whose atmospheric concentration increases with time and which is readily dissolved in the upper ocean. Inventories of this "transient surface tracer" (TST) help to quantify the efficiency of ventilation and interpret distributions of such realistic tracers as CFCs, SF_6 and tritium. This study uses an offline tracer model, described in Section 2, to simulate distribution of these tracers. Sections 3 and 4 discuss simulations of the BIR and TST tracers, with and without mesoscale eddies, and the direct role of mesoscale eddies in ventilation of the Southern Ocean. Discussions and conclusions are presented in Section 5.

2 Southern Ocean Offline Tracer Model – SOOTM

The Southern Ocean Offline Tracer Model (SOOTM) uses pre-calculated velocities and layer thicknesses to solve the tracer equation. These variables were calculated in a separate "base" simulation with the HYbrid Coordinate Ocean Model (HYCOM; *Bleck*, 2002; *Chassigent et al*, 2003; *Halliwell*, 2004). HYCOM is based on the Miami Isopycnic Ocean Model (MICOM; *Bleck et al*, 1992, *Bleck and Chassignet*, 1994) and uses isopycnal coordinates in the open ocean and below the mixed layer. Main advantages of formulation in isopycnic coordinates include the absence of spurious numerically diapycnal mixing, which prevents unrealistic dilution of subsurface water mass properties – a chronic problem of z-coordinate models (e.g. *Griffies et al.* 2000),

and most efficient resolution of the baroclinic structure. HYCOM's coordinate system dynamically transitions to other coordinate types (sigma- and z-coordinates) to provide optimal resolution in the surface mixed layer, in high-latitude unstratified regions, and near coasts.

The base simulation that SOOTM is based on has a global domain with 1/12^{o} spatial resolution; the horizontal grid is rectilinear south of 47^{o}N (being equatorial Mercator except in the high southern latitudes) followed by an Arctic bipolar patch. The vertical grid has 32 hybrid layers (isopycnal in the deep ocean, z levels in the ocean interior near the surface, and sigma coordinates near the coasts). The horizontal resolution (~ 3.2–8km at 70^{o}S-30^{o}S) is among the highest available today, but still falls short of accurate resolution of the small-scale eddies of the size of the first internal Rossby deformation radius (~10-20 km at these latitudes; *Chelton et al.* 1998). Our focus is, therefore, on eddies with scales of larger than approximately 20-50 km. The potential density is referenced to the 20-MPa surface, and the model's equation of state has thermobaric corrections indicated (*Sun et al*, 1999, *Chassignet et al*, 2003). The model has a KPP parameterization for vertical mixing (*Large et al*, 1994).

The spinup for the base calculation was completed at the Naval Research Laboratory (NRL) starting from the observed stratification. The model was forced with monthly ECMWF (ERA40) forcing fields plus 6-hourly anomalies obtained from NOGAPS winds. A simple "energy loan" ice model is included, without advection or dynamics. At this resolution, the model has been used extensively at NRL. Typically a climatological spin up is used to initialize inter-annual simulations; see http://www.hycom.org for more detail. The pre-calculated fields needed for our offline model come from a separate on-line regional simulation of the Southern Ocean, initialized from the HYCOM global climatological run and integrated for 5 years and 2 days. Separate

integration was required because the standard HYCOM run did not save instantaneous layer thickness fields. Surface boundary conditions and other parameters in this regional simulation are identical to those in the global climatological run. The latitudinal domain of SOOTM extends from 78.6°S to 20°S. At the northern boundary temperature, salinity and layer thickness are relaxed to global climatology; this relaxation helps to keep stratification and circulation at the northern boundary close to their values in the global simulation. The Indonesian Throughflow is not included in this regional simulation, which can influence upper-ocean tracer distributions and ACC currents. We did not, however, detect a trend in the ACC transport south of Australia.

The off-line tracer approach was originally formulated by R. Bleck (personal communication); early off-line tracer simulations are presented in *Sun and Bleck* (2001). The off-line tracer model solves the prognostic equation for the tracer concentration c within an n^{th} hybrid layer of thickness $\Delta z(x,y,t)$:

$$\frac{\partial(c_n \Delta z_n)}{\partial t} = -\nabla \cdot (c_n \boldsymbol{U}_n) - (\omega_t c_t - \omega_b c_b) + A_h \nabla \cdot \nabla c_n \Delta z_n \qquad (1)$$

where $\boldsymbol{U}=\boldsymbol{u}\Delta z$ is the horizontal volume flux within each layer, ω stands for the vertical velocity through each layer, subscript "n" denotes the layer number, and subscripts "t" and "b" denote properties at the top and bottom of this layer respectively. The continuity of volume within each layer requires

$$\omega_t - \omega_b = -\nabla \cdot (\boldsymbol{U}_n) - \frac{\partial \Delta z_n}{\partial t} \qquad (2)$$

Daily-mean values of $\boldsymbol{U}$ are used to compute the first terms on the right-hand sides of (1) and (2), whereas the change in the layer thickness (second term on the right-hand side of Equation 2) is calculated from the instantaneous daily layer thicknesses. The conservation of mass is, there-

fore, exact in the daily mean sense. A_h is the horizontal Laplacian diffusivity required for numerical stability; its value is 0.01 m $sec^{-1} \cdot \Delta x$ in the control simulation, with Δx being the horizontal grid spacing. Equation 1 is solved using a three-dimensional, fourth-order advection scheme with flux-corrected transport (*Zalesak*, 1979). The time step is 1 hour.

The goal of this study is to determine the relative importance of mesoscale advection in ventilation of the ocean below the mixed layer. For this purpose, the tracers described in the next section are injected into the ocean interior at the base of the mixed layer and advected by the three-dimensional circulation. The model is thus used in a semi-idealized mode with the KPP scheme turned off and tracers instantaneously homogenized with the mixed layer. Note that diapycnal tracer fluxes below the mixed layer are retained due to the conservation of mass (Equation 2).

The offline simulations discussed in the following section are carried out using velocities, layer thicknesses and mixed layer depth taken from the online simulation that was carried out for 5 years and 2 extra days ("online fields" hereafter). These online fields are recycled at the end of each 5-year period to produce the extended time series of these fields. To reduce the shock at the end of each 5-year cycle, all online fields at Day 1 at online Year 1 are replaced by the online fields averaged between Day 1 at online Years 1 and 6; the same was done for Day 2. Note that this method of "recycling" the physical fields does not guarantee strict conservation of tracer in each layer; we also tested a method in which the tracer inventory in each layer is conserved at the time of the recycling, by multiplying the tracer concentrations at Day 1 of Year 6 by the ratio between Δz at Day 1 Year 6 and Day 366 Year 5, and found the results to be very similar in both cases.

In addition to the control simulations (FULL_ADV), we carried out the simulation MEAN_ADV, in which the mesoscale variability is removed from $\boldsymbol{U}$ and layer thicknesses Δz by time-averaging; the resulting variables $<\boldsymbol{U}>$ and $<\Delta z>$ are referred to as the "mean fields". Defining mesoscale anomalies as deviations from the mean, $\boldsymbol{U}' = \boldsymbol{U} - \langle \boldsymbol{U} \rangle,\ \Delta z' = \Delta z - \langle \Delta z \rangle$, we can rewrite the tracer balance equation in the following form

$$\frac{\partial (c_n \Delta z_n)}{\partial t} = \overbrace{-\nabla \cdot (c_n \boldsymbol{U}_n{}') - (\omega_t{}' c_t - \omega_b{}' c_b)}^{eddy\ advection} \overbrace{-\nabla \cdot (c_n \langle \boldsymbol{U}_n \rangle) - (\langle \omega_t \rangle c_t - \langle \omega_b \rangle c_b)}^{mean\ advection} + A_h \nabla \cdot \nabla c_n \Delta z_n \quad (3)$$

Note that we choose not to decompose the tracer layer inventory $c\Delta z$ into the mean and eddy parts here, because this study examines transient tracers whose time averages may not be meaningful (see below).

Two definitions of the mean field were considered: 1) climatological annual cycle; and 2) long-term time average. In Method 1, the climatological annual cycle of each field is calculated by first averaging each daily quantity over its value on the same day in 5 different years, and then low-pass filtering the result in time, using a 50-day sliding mean. Because only 5 years are available for this method and because mesoscale eddies are often characterized by time scales of a few months, the annual cycle in Method 1 appears to be contaminated by mesoscale variability, particularly in the Agulhas region. In contrast, Method 2 effectively removes mesoscale features, but the annual cycle is removed as well. We chose Method 2 for all advective terms, but verified that results do not change qualitatively if Method 1 is used instead. The lack of the annual cycle in the mixed layer depth (and its winter-time deepening) would, however, strongly impact the tracer injection rate from the mixed layer into the ocean interior. To alleviate this effect, we use

Method 1 to remove mesoscale variability in the mixed-layer depth in MEAN_ADV. MEAN_ADV is, therefore, the case with stationary mean circulation below the mixed layer and seasonally varying tracer injection rate.

2.1 Test of the offline advection

To estimate the error due to the use of daily values in the offline calculations of the advective terms, we carried out on-line simulations of idealized tracer patches in the upper ocean and compared the results to the SOOTM simulations of the same tracer. The tracer in the model is initialized with two rectangular, uniform patches in the top 15 layers; one patch in the Pacific and another – in the Atlantic sectors of the Southern Ocean (*Figure 1*); there are no internal sources and surface fluxes. The simulation is run for approximately 6.5 months, and at the end of the run both patches are displaced by the mean advection and distorted by the eddying flow. The upper layers were chosen because of large horizontal velocities; note also that this is a rather strict test of the offline algorithm because of very sharp gradients at the patch edges.

The distributions in the online and offline simulations remain visually indistinguishable throughout the entire simulation. To quantify the errors in the dispersion and advection of the tracer, we analyze the position of the "center of mass" of each patch (X,Y) and the tracer dispersion D relative to (X,Y) in each n^{th} layer by:

$$X_n = \int c_n(x,y,t)xdxdy \left\{ \int c_n(x,y,t)dxdy \right\}^{-1},$$

$$Y_n = \int c_n(x,y,t)ydxdy \left\{ \int c_n(x,y,t)dxdy \right\}^{-1}$$

$$D_n = \int c_n(x,y,t)\{(x-X)^2 + (y-Y)^2\}\,dxdy \left\{\int c_n(x,y,t)dxdy\right\}^{-1} \quad 4)$$

The errors, defined as the difference between online and offline values of X,Y and D, are nearly uniform in the upper 13 layers, tend to be larger in layers 14-15 and are hard to quantify for the deep ocean due to very low concentrations of the tracer. For the Pacific (Atlantic) patch, the errors in X and Y, rounded to the tenth of a degree (approximate grid spacing), are 0.0-0.4 (0.0-0.4) and 0.0 (0.1) degrees respectively. Relative to the change in X and Y from the initial positions, these errors are less than 3.0 (0.4) and 0 (1.7) per cent respectively. The errors in D are less than 2.0 and 1.7 per cent for the Pacific and Atlantic patches respectively. We conclude that the errors due to the use of daily fields are sufficiently small to warrant the use of SOOTM for simulations of the passive tracers.

3 Boundary Impulse Response Tracer

The main goal of this part of the study is to examine the relative importance of the mean and mesoscale advection in establishing communication between the mixed layer of the ACC and the oceanic interior. For this purpose, the BIR tracer is set to unity within the region of the topmost model layer ("surface") of the ACC (south of 45^{o}S) and for 1 year, and then reset to 0 in the same layer afterwards. Simulations with the entire surface being the source region have also been carried out and led to qualitatively similar results; these results are only briefly discussed where appropriate. The tracer is then ejected from the mixed layer into the deeper layers through the mixed-layer entrainment, diapycnal mass fluxes and along-isopycnal advection. Below the surface, the tracer is conserved and satisfies Equations (1-2). After Year 1, the entire surface mixed

layer becomes a sink for the tracer, and the BIR concentrations begin to decline approaching zero after sufficiently long time. The long-term time mean of BIR concentration is zero.

In a simple case of one-dimensional steady advection, BIR concentrations have a form of a propagating pulse. The inventory of the BIR tracer in any given region initially increases (as the pulse enters the region), then stays constant (as the pulse propagates inside the region), and finally declines (as the pulse leaves the region). Complex three-dimensional flow and the eddy-induced mixing in this study causes spreading of this pulse in both space and time (e.g. *Holzer and Hall* 2000). For example, the along-isopycnal eddy mixing in the ACC will contribute to the BIR-tracer transport from the mixed layer into the subtropical gyres, while the eddy-induced mixing with surrounding waters will also dilute the subtropical BIR concentrations and spread the tracer away from the mean pathways. This transient behavior informs us on how the advection communicates the information from the mixed layer to the subsurface ocean and on what the corresponding pathways and timescales are. Note that we do not attempt to produce statistically meaningful TTD, which would require an ensemble of BIRs (*Maltrud et al.* 2010); our analysis of two simulations differing by the start year in the 5-year cycle, however, showed very similar results.

3.1 Pacific Sector

The tracer accumulates in the mixed layer of the South Pacific throughout the first year (not shown), and large tracer inventories are observed in the western part of the South Pacific sector, where the mixed layer is the deepest and where SAMW forms. From this region and below the mixed layer, the tracer is advected eastward into the rest of the Pacific sector (Figure 2a-c). By Year 5, the tracer patch is centered in the middle of the basin (at approximately 120^{o}W; see also

Figure 2c), and by Year 10, the center of mass of the Pacific tracer patch is off South America (Figure 2d). Equatorward spreading of the tracer is slow, and the BIR signal reaches 30^{o}S only by the end of the first decade (Figure 2d). Both the accumulation of the tracer at 90^{o}W by the end of the first decade and slow decrease in the tracer concentrations during the second and third decades indicate a long tail in the distribution of the ventilation timescales (not shown). This wide shape of the BIR distribution is typical for flows with complex spatial structure and active eddy stirring (*Holzer and Hall* 2000).

In the absence of eddy stirring, the tracer is concentrated along the mean advective pathways (Figure *3*a-c). For example, the largest concentrations at Year 3 are found in two narrow bands: one zonal band is centered at 45^{o}S and another one is horizontally slanted and extends eastward from the coast of New Zealand. The northern band in MEAN_ADV is slowly advected north-eastward (Figure *3*c-d) by the subtropical gyre, whereas the southern elongated patch is carried by the ACC toward the South American coast. After encountering the continent, the latter patch propagates northward, reaches the northern part of the subtropical gyre and moves westward. The circulation of these patches in the subtropical gyre is further illustrated in Figure 4c, which shows the Hovmoller diagram of the meridionally-averaged (between 50°S and 20°S) tracer. The evolution of the BIR tracer in MEAN_ADV is noticeably different from the FULL_ADV simulation where these two pathways are blended together by the eddy-induced stirring (Figure 2 and Figure 3). At 65-50°S (Figure 4d), the BIR tracer in MEAN_ADV propagates along ACC, entering the Pacific from the Indian sector at approximately Year 10 (see also Figure 3d); the same pathway is not observed in FULL_ADV (fig.4b). Another difference can be seen near New Zealand (Figure 2a-c and Figure *3*a-c) where eddies have been shown to enhance ventilation (*Hartin et al.* 2011).

283 The relative importance of the mean advection and eddy-induced stirring in FULL_ADV is
284 further illustrated by the divergence of the tracer fluxes, namely the terms “mean advection” and
285 “eddy advection” in Equation 3, as well as their sum, “full advection”. Annual averages of these
286 fields (Figure 5d,g,j) demonstrate a central role of the mean advection, which dominates the full
287 advection starting at Year 5. In particular, slow decline of tracer concentrations in the ACC re-
288 gion (south of approximately 45^{o}S) and the penetration of the signal into the northern part of the
289 domain at Year 10 are primarily explained by the mean currents. Eddy-induced stirring resists
290 this tendency near the northern edge of the ACC, but the magnitudes of the eddy advection term
291 are small.

292 Equatorward spreading of the BIR tracer takes place primarily along isopycnal surfaces. This
293 process corresponds to the subduction and formation of AAIW, and is illustrated by the zonally
294 averaged BIR concentrations (Figure 6, left column). By year 10, most of the tracer is outside of
295 ACC (north of 45^{o}S in Figure 6e) and this cross-ACC transport is facilitated by eddies. The max-
296 imum of the zonal-mean tracer patch is sliding between along the $\sigma_\theta = 27.05$ kg m^{-3}; most of the
297 tracer found in the $\sigma_\theta = 26.8 – 27.4$ kg m^{-3} range, which corresponds to SAMW/AAIW (e.g. *Har-*
298 *tin et al.* 2011). The S=34.4 isohaline (not shown), also traditionally used for defining the lower
299 boundary of AAIW, is more shallow than the $\sigma_\theta = 27.4$ kg m^{-3}, which is explained by a warm bi-
300 as in this simulation. This BIR tracer patch also extends into the deeper ACC layers ($\sigma_\theta > 27.4$),
301 where the tracer stays throughout the duration of the experiment, and into shallow layers (σ_θ
302 <26.8 kg m^{-3}), where the northward spreading is faster than within the AAIW layer.

303 The along-isopycnal penetration in FULL_ADV is facilitated by the eddy-driven mixing and
304 is clearly a result of the full three-dimensional flow within the ACC (*Pennel and Kamenkovich*

2014). The BIR pulse in MEAN_ADV does not follow the isopycnals within the ACC (south of 45°S) and is considerably shallower. The main ventilation pathway in MEAN_ADV is approximately at the σ_θ = 26.8 isopycnal, as is illustrated by a concentrated tracer pulse (Figure 4c and Figure 6, right column) that is moving with the subtropical gyre along the South American coast. The meridional propagation of the center of this patch is faster than in FULL_ADV, due to a shallower trajectory in MEAN_ADV. However, the eddy stirring in FULL_ADV causes pulse widening (*Holzer and Hall* 2000), which facilitates northward tracer spreading (Figure 6g,h). Note that the high tracer concentrations in MEAN_ADV are observed within ACC at Year 10 (Figure 6f), but not at Year 20, which is explained by the tracer leaving the Pacific sector at the end of the second decade (Figure 4d).

Ventilation timescales of AAIW are studied by calculating the evolution of the BIR inventories within the AAIW layer in the 35°S-30°S latitude range. AAIW is defined here by waters with either σ_θ=27.05-27.4 kg m^{-3} or salinities between 32.2-32.4 ppt. The peak values in FULL_ADV are reached by the middle of the second decade (Figure 7a), after which time the BIR tracer inventories in this region begin to decline, forming a long tail with large values even at the end of the third decade. Most of the BIR tracer is contained within AAIW (Figure 7b) for the entire length of the simulation, which highlights the importance of AAIW in the ventilation of the Pacific subtropical gyre. The pulse is more concentrated in time in MEAN_ADV, which is expected in the absence of eddies, as discussed earlier. The passing of the peak is observed at approximately the same time in both simulations, but the BIR tracer begins to fill the AAIW layer in FULL_ADV at much earlier times than in MEAN_ADV. The latter fact demonstrates that the eddy-induced northward transport accelerates ventilation of the AAIW layer (see also *Hartin et al.* 2014). The most striking difference between FULL_ADV and MEAN_ADV is in much

larger (by more than 50%) peak values in BIR inventories in the latter case. This difference is in large part associated with the arrival of the BIR pulse from the Indian into the Pacific sector of the Southern Ocean at approximately Year 10 (Figure *3*d and Figure 4d) in MEAN_ADV; this pulse then propagates northward within the subtropical gyre. As is discussed in Section 3.2 below, this Indian-to-Pacific tracer transport is weakened in FULL_ADV by the eddy-induced removal of tracer from the ACC. The fraction of the BIR tracer contained within the AAIW layer is, however, higher in MEAN_ADV than in FULL_ADV during the third decade. This is due to the fact that the BIR tracer in MEAN_ADV is found at shallower depth than in the FULL_ADV.

3.2 Atlantic and Indian Sectors

Initially, the BIR tracer enters the South Atlantic primarily from the eastern South Pacific and from the deep mixed layer downstream of the Drake Passage (Figure 2a). The tracer then becomes entrained into the northward-flowing Malvinas Current and enters the southern branch of the subtropical gyre. By Year 3, there is a pronounced maximum in the tracer concentration in the western South Atlantic (Figure 2b), whereas the tracer upstream of the Drake Passage is significantly depleted. The geographical distribution of tracer inventories in MEAN_ADV are still very similar to FULL_ADV at this time (Figure *3*a-b), which indicates the dominant role of the mean advection at the initial stages of ventilation.

Mean advection continues to play an important role in distribution of the BIR tracer at later times. The corresponding mean pathways are illustrated by the MEAN_ADV simulation, in which the eddy-induced tracer spreading is turned off. The southward-flowing Brazil Current acts to block further northward penetration of the signal by the Malvinas Current and to keep the tracer within the ACC, which then washes the tracer away from the Atlantic sector (Figure 3c-d).

During the first decade, the BIR tracer in MEAN_ADV is concentrated within a zonally elongated patch centered at approximately 45°S (Figure *3*c-d), which propagates from the Atlantic into the Indian sector of the ACC at the speed of approximately 0.05 m sec^{-1} (Figure 3b-e and Figure 4d). At Year 10, this tracer patch is located south of Australia. The patch then passes south of New Zealand and enters the Pacific sector of the ACC (Figure *3*e and Figure 4d).

Starting at the end of Year 3, the importance of eddy-driven advection becomes pronounced. The tracer is dispersed by eddies from the mean ACC pathways and eventually fills the Atlantic and Indian sectors equatorward to 30°S (Figure 2c-e). As a result of this eddy-induced spreading and in contrast to MEAN_ADV, significant amounts of tracer in FULL_ADV are found further equatorward in the Atlantic subtropical gyre and are prevented from entering the Indian sector by the African continent (Figure 2d). As a result, the total tracer inventory in the Atlantic north of 45°S in FULL_ADV is higher than in MEAN_ADV, with high concentrations in the eastern South Atlantic in both runs (Figure 2d and Figure 3d). Further downstream, similar effects of eddies are observed in the Indian Ocean, where the BIR tracer in FULL_ADV is found further north in comparison to MEAN_ADV (Figure 2d and Figure 3d). The eddy-induced spreading, therefore, acts to isolate the South Pacific from the upstream influence of the Atlantic and Indian sectors of the Southern Ocean.

As in the Pacific sector, the mean advection dominates tracer evolution in the Atlantic and Indian sectors of the ACC (south of 45°S), especially the tracer transport from the Atlantic into the Indian sector during Years 5-10 (Figure 5e-f and h-i). This zonal transport is illustrated by the negative (positive) full advection terms (black lines) in the Atlantic (Indian) sectors. The eddy advection terms (blue lines) act to compensate for these changes, but their magnitudes are

much smaller than those of the mean advection (red lines). North of the ACC, the eddy advection is comparable in magnitude to the mean advection, and the eddy-induced tracer transport is northward across approximately 40^{o}S (Figure 5 e, f, h, i, k). This meridional transport is due to eddy-induced stirring and is important in spreading the tracer and retaining it in the Atlantic and Indian sectors.

The ventilation of the Atlantic basin is further illustrated by the latitude-depth plots of zonally averaged BIR values (Figure 8). As in the Pacific sector, the BIR pulse in FULL_ADV is advected by the mean currents, but is also spreading vertically and horizontally, due to cross-isopycnal fluxes and eddy-induced mixing. The vertical spreading is, however, deeper than in the Pacific sector. After leaving the ACC, the center of the tracer pulse in FULL_ADV is moving roughly along σ_θ=27.4 kg m^{-3} and is found at 40^{o}S by the end of the first decade (Figure 8e) and at 27^{o}S by the end of the second decade (Figure 8g). Although the pulse center propagates with approximately the same speed in FULL_ADV and MEAN_ADV, eddies have significant effects on the ventilation of the Atlantic sector of the Southern Ocean. These effects are most pronounced in the distribution of the BIR tracer at the end of the second decade (Figure 8g,h).

First, larger amounts of the BIR tracer remain within ACC in MEAN_ADV than in FULL_ADV (Figure 2e and Figure *3*e), which implies that the ventilation by the mean currents is significantly weaker and slower in the absence of eddies. Interestingly, these effects are more pronounced in the Atlantic than in the Pacific sectors (Figure 6g,h and Figure 8g,h). This difference between the Pacific and Atlantic basins is explained by the difference in geometry. The South American continent effectively blocks the eastward spreading of the tracer within the ACC, thus facilitating its equatorward propagation by the mean currents in the eastern Pacific.

394 The Australian and African continents are located further northward and cannot have an equally
395 strong effect on tracer distribution. Second, as in the Pacific sector, the tracer spreading in
396 FULL_ADV is along sloping isopycnals, whereas in MEAN_ADV the tracer transport is more
397 horizontal. As a result, the tracer penetrates deeper in FULL_ADV than in MEAN_ADV.

398 BIR inventories in the AAIW layer (waters with either σ_θ=27.05-27.4 kg m^{-3} or S=32.2-32.4
399 ppt) reach peak values at year 6 in FULL_ADV (Figure 7c), which is much earlier than in the
400 Pacific. This rapid ventilation is associated with the western part of the South Atlantic (Figure
401 2a-b), where the tracer first accumulates and then is carried northward by the Malvinas Current
402 and spreads due to eddy-induced mixing. The AAIW inventories and the fraction of the total BIR
403 inventory they correspond to both decline steadily at later times (Figure 7c,d). AAIW ventilation
404 in MEAN_ADV is significantly weaker and slower than in FULL_ADV, and the peak values in
405 the absence of eddies are achieved during the second decade. Eddy-induced spreading clearly
406 facilitates ventilation of the South Atlantic and prevents tracer from leaving the basin within
407 ACC. Note, however, that most of the BIR tracer in MEAN_ADV, is contained within the
408 AAIW layer, whereas most of the tracer in FULL_ADV is concentrated below the AAIW layer.
409 This is a consequence of deeper penetration of the BIR tracer in the latter case. In the experi-
410 ments with BIR having a source in the entire surface, the evolution of its AAIW inventory is
411 very similar (not shown).

412 # 4 Transient Surface Tracer

413 Transient Surface Tracer (TST) is an idealized analog of a transient tracer whose atmospheric
414 concentrations are increasing with time (e.g. CFC and SF6), and which is absorbed and redistrib-
415 uted in the ocean as a passive tracer. TST, therefore, can help to interpret distribution of these

tracers in numerical simulations and observations. This tracer can be derived from the "entire surface" BIR tracer calculated in this study and shares main features discussed in the previous section; only a brief discussion is given here. Below the surface, TST is conserved and satisfies equation (1). The tracer is uniformly distributed in the uppermost model layer ("surface") and its concentration c_S is increasing linearly with time t that has passed since the beginning of the integration, $c_s = t$ (time is in years). In this sense, TST is different from, for example, CFC, whose surface concentrations decrease toward the equator. TST is also related to the ideal age tracer, which is widely used for the studies of the oceanic water masses (e.g. *England* 1993). In particular, the quantity $t - c_s(t)$, would be equivalent to the idealized age τ_{age}, if the integration of the ensemble of runs were carried out to equilibrium and this quantity reaches a constant. The latter property implies that $c_s(t) \to t - \tau_{age}$ in the long-time limit, and TST would exhibit linear growth.

In FULL_ADV, the TST distribution within ACC (south of 45°S) is primarily along the isopycnal surfaces (Figure 9); this is particularly evident in the Pacific sector. Interestingly, the along-isopycnal distribution of TST appears to be nearly uniform within the ACC, despite the linear increase in TST concentrations at the surface. The eddy-induced isopycnal diffusion is, therefore, sufficiently strong to make the along-isopycnal tracer anomalies smaller than the average tracer value. In the case of TST, this means that the time that has passed since the beginning of the experiment is much longer than the diffusive time scale. The latter time-scale can be estimated by $T = \frac{{L_y}^2}{k_y}$, where L_y is the meridional length scale and k_y is the meridional eddy diffusivity. Taking L_y=200km and k_y =1000 m^2sec^{-1} (e.g. *Abernathey et al.* 2010) yields T≈3 years, which is in general agreement with the along-isopycnal sliding of the BIR pulse (Figure 6)

438 and is an order of magnitude shorter than 30 years. In the absence of eddies, in contrast,
439 MEAN_ADV exhibits a shallower TST distribution, with large along-isopycnal gradients. As is
440 demonstrated in Section 3, the ventilation signal in MEAN_ADV moves along a trajectory that is
441 shallower than in FULL_ADV and does not follow the main isopycnals.

442 The TST model output after 30 years can be compared with observed distributions of CFC,
443 for example WOCE section P16 along 150°W in South Pacific (http://woceatlas.ucsd.edu),
444 despite the differences between TST and CFC discussed above. It is clear that FULL_ADV
445 (Figure 9a) is more similar to observations than the MEAN_ADV (fig.8b). The CFC-12 data and
446 FULL_ADV model both show tracer reaching to 2500m at 50°S and shoaling toward 1000m at
447 30°S, not in MEAN_ADV case. The agreement in South Atlantic is less convincing. Both
448 FULL_ADV and observations (for example WOCE section A16 along 25°W) show tracer
449 penetration reaching below 1500m north of the ACC (45°S-30°S), which is considerably deeper
450 than the TST penetration in South Pacific or in MEAN_ADV Atlantic. In contrast to the
451 observed CFC-11 distributions, however, small concentrations of TST in FULL_ADV are found
452 at even greater depths, up to 2500m. The causes of this difference with observations remain
453 unclear.

454 As a result of the deeper eddy-driven ventilation, the TST inventories in the ACC are
455 noticeably larger (up to 50%) in FULL_ADV than in MEAN_ADV simulations (Figure 10). In
456 the Pacific sector of the Southern Ocean, this difference is, however, smaller north of the ACC,
457 which signifies the importance of the mean large-scale advection and local ventilation. In the
458 Atlantic-Indian sector, the TST inventories in FULL_ADV are consistently larger than in
459 MEAN_ADV everywhere north of 50°S. Maximum inventories in this sector are observed at

approximately 40°S in both simulations (Figure 10d). Stronger ventilation within the ACC explains approximately half of the difference between FULL_ADV and MEAN_ADV north of 45°S. This is suggested by a cursory comparison between our standard BIR simulation (source region in ACC, south of 45°S) and the BIR forced from the entire surface (not shown). This comparison also suggests an important role of the Indian Ocean and the Agulhas Leakage in distribution of TST in the Atlantic-Indian sector. *Wang et al.* (2014) studied spreading of Agulhas waters into the Southern Ocean and found that although most of these waters end up in the Indian sector, a significant portion enters the South Atlantic through the boundary current along the southern tip of South Africa and via Agulhas rings. These processes are, however, outside of the scope of this paper and detailed analysis is not attempted here.

5 Discussion and Conclusions

This study examines the relative importance of the mean currents and mesoscale eddies in the ventilation of the upper Southern Ocean, with the ventilation defined as property exchange between the mixed layer and the ocean below. The study employs a new offline tracer model, which uses pre-calculated velocities to advect dynamically passive tracers, that is, tracers that do not themselves affect velocities and mixing. The computational efficiency of this approach permits multiple extended high-resolution simulations of oceanic tracers. Two idealized tracers are considered here: the BIR tracer, which helps to determine the time and pathways for ventilation of the subsurface ocean from a given region of the surface mixed layer, and the TST that mimics distribution of a transient tracer whose atmospheric concentrations are increasing in time. Another advantage of the offline formulation is in its convenience of running sensitivity experiments with modified advection. In this study, contrasting the control simulation

(FULL_ADV) and a simulation without mesoscale eddies (MEAN_ADV) helps to separate the direct effects of the mean advection and eddy-induced stirring.

The analysis reveals complex three-dimensional ventilation pathways at the level corresponding to AAIW, controlled by the interplay between the mean advection and eddy-induced mixing. The main mean pathway is due to the eastward advection within the ACC; it is partially obstructed by the South American continent, which directs a portion of the surface-forced signal with the South Pacific subtropical gyre. This process facilitates formation of the AAIW in the eastern South Pacific. East of the South American continent, a BIR tracer pulse propagates along a wide zonal pathway within ACC that links the South Atlantic, Indian and Pacific oceans. In MEAN_ADV, this pulse ends up in the South Pacific and increases the ages of AAIW; only small amounts of the BIR tracers are retained in the Atlantic and Indian sectors. Although the Malvinas Current in the western South Atlantic transports the tracer northward, the southward-flowing Brazil Current acts to block this penetration of the signal and keep the tracer within ACC.

The eddy-induced advection has two main effects on the ventilation. Firstly, the eddies act to remove the tracer away from the mean pathways of the ACC, resulting in equatorward penetration of the BIR pulse into the South Atlantic, Indian and Pacific oceans. As a result, the tracer is effectively retained in these basins, since its eastward propagation is partially blocked by the African, Australian and South American continents. Thus, there is enhanced ventilation of the subtropical gyres. This effect is most significant in the South Atlantic and Indian regions, which is confirmed by our analysis of the tracer flux divergence. Secondly, the eddies facilitate along-isopycnal spreading of the tracer, and this effect is most pronounced within the ACC. In the

absence of eddies, the spreading of tracers is more horizontal and cross-isopycnal, which demonstrates that the along-isopycnal tracer transport is a result of the three-dimensional interplay between eddies and mean advection. This eddy-induced spreading also results in larger inventories of TST within ACC, as well as in the South Atlantic, Indian and Pacific basins. If the eddy stirring is sufficiently strong, it also homogenizes TST along the mean isopycnals, despite continuously increasing surface concentrations.

This study has several implications for interpretation of observational data and numerical simulations. The results suggest that AAIW in the Pacific is a mix of relatively young, locally subducted waters and older waters brought in by ACC from the Atlantic and Indian sectors. The action of eddies inhibits the latter source, decreasing the age of the Pacific AAIW. Biases in representation of eddies (either explicitly simulated or parameterized) will, therefore, lead to biases in the average age and composition of this water mass. On the other hand, mean currents are clearly important. The formation of AAIW is governed by the mean subduction in the South Pacific, and the Malvinas and Brazil currents confluence and circulation in the eastern South Atlantic play an important role in the ventilation of the South Atlantic Ocean. This is encouraging for climate models that lack spatial resolution for accurate representation of mesoscale currents, assuming that the mean circulation are sufficiently realistic and parameterized eddy transports are strong in these simulations.

The direct validation of eddy parameterization schemes is, however, a challenging task and is not attempted here. A comparison between FULL_ADV and MEAN_ADV cannot be easily used for this purpose, mainly because the mean circulation and stratification are different between high- and low-resolution simulations. Many significant effects of eddy advection in this study are

526 also observed north of the Drake Passage, where the circulation is inherently three-dimensional
527 and the convenient formalism of the two-dimensional Transformed Eulerian Mean and residual
528 overturning (*Andrews and McIntyre* 1976; *Marshall and Radko* 2003; *Henning and Vallis* 2005)
529 is not directly applicable. This study defines mean fields by time averaging, which is effective in
530 removing mesoscale variability from velocities and stratification, but cannot lead to a meaningful
531 definition of the mean value for transient tracers; for example, time average of the BIR tracer
532 approaches zero at very long times. This further complicates the conventional Reynolds
533 decomposition in this study; tracers in a statistically steady state would be required for this
534 purpose. Analysis of MEAN_ADV with parameterized eddies can, however, address an
535 important question of what properties of eddy transport must be captured by a parameterization
536 scheme and what properties of this transport are less important. Such analysis, which requires an
537 estimate of location-dependent parameters of a parameterization scheme (such as the isopycnal
538 diffusivity tensor) in the realistic Southern Ocean domain, is planned for the future.

539 Although the offline simulations cannot be directly applied to dynamically active tracers, the
540 propagation of the signal from the surface into the ocean interior can be useful for understanding
541 evolution of the heat, salt and buoyancy anomalies. For example, fast communication between
542 the surface and western South Atlantic can have implications for the variability of the Atlantic
543 Meridional Overturning Circulation (AMOC), since the stratification in this region controls the
544 AMOC intensity (*Kamenkovich and Radko* 2011). Further studies of the ventilation mechanisms
545 should involve realistic tracers with spatial and temporal variability at the surface.

546 *Acknowledgements* The authors are grateful to two anonymous reviewers for their helpful
547 suggestions on improving this manuscript. This study was supported by NSF grant OCE-

1060163. IK was in part supported by NSF's Southern Ocean Carbon and Climate Observations and Modeling (SOCCOM) project under the NSF award PLR-1425989, with additional support from NOAA and NASA; RAF was in part supported by NSF award OCE-1433922. We would like to thank Dr. Joseph Metzger for his help in preparing the online simulations. CFC distributions along WOCE sections were downloaded from the online WOCE Atlas (http://woceatlas.ucsd.edu). All data from numerical simulations are available upon request from ikamenkovich@miami.edu.

6 REFERENCES

Abernathey, R., J. Marshall, and M. Mazloff, 2010: Enhancement of mesoscale eddy stirring at steering levels in the Southern Ocean, *J. Phys. Oceanogr.,* **40**, 170-184.

Andrews, D.G., and M.E. McIntire, 1976: Planetary waves in horizontal and vertical shear: The generalized Eliassen-Palm relations and the mean zonal acceleration. *J. Atmos. Sci.*, **33**, 2031-2048.

Bleck, R., and E.P. Chassignet, 1994. Simulating the oceanic circulation with isopycnic coordinate models. *The Oceans: Physiochemical Dynamics and Resources*. The Pennsylvania Academy of Science, 17-39.

Bleck, R., Rooth, C., Hu, D., Smith, L., 1992: Salinity-driven thermocline transients in a wind- and thermohaline-forced isopycnic coordinate model of the North Atlantic, *J. Phys. Oceanogr.*, **22**, 1486-1505.

Bleck, R., 2002: An oceanic general circulation model framed in hybrid isopycnic-cartesian coordinates. *Ocean Modelling*, **4**, 55-88.

Booth, J. and I. Kamenkovich, 2008: Isolating the role of transient mesoscale eddies in mixing of a passive tracer in an eddy resolving model, *J. Geophys. Res.,* **113**, C05021, doi:10.1029/2007JC004510.

Chassignet, E.P., L.T. Smith, G.R. Halliwell, and R. Bleck, 2003: North Atlantic simulation with the HYbrid Coordinate Ocean Model (HYCOM): Impact of the vertical coordinate choice, reference density, and thermobaricity. *J. Phys. Oceanogr.*, **33**, 2504-2526.

Chelton, D. B., R. A. de Szoeke, M. G. Schlax, K. El Naggar and N. Siwertz, 1998: Geographical variability of the first-baroclinic Rossby radius of deformation. J. Phys. Oceanogr., **28**, 433–460.

England, M.H., 1995: Using chlorofluorocarbons to access ocean climate models, *Geophys. Res. Lett*., **22**, 3051-3054.

England, M. H., 1993: South Atlantic Ocean Ventilation: a numerical model study with geochemical tracers. *Ann. Geophys.*, **11**, Suppl. II, C163.

Frölicher, T. L**.**, J. L. Sarmiento, D. J. Paynter, J. P. Dunne, J. P. Krasting, M. Winton, 2015, Dominance of the Southern Ocean in anthropogenic carbon and heat uptake in CMIP5 models. *J. Climate,* **28**, 862-886.

Griffies, S. M., R. Pacanowski, and R. Hallberg, 2000: Spurious diapycnal mixing associated with advection in a Z-coordinate ocean model, *Mon. Wea. Rev*., 128, 538-564.

Gruber, N. , M. Gloor, S. E. Mikaloff Fletcher, S. Dutkiewicz, M. Follows, S. C. Doney, M. Gerber, A. R. Jacobson, K. Lindsay, D. Menemenlis, A. Mouchet, S. A. Mueller, J. L. Sarmiento, and T. Takahashi, 2009: Oceanic sources and sinks for atmospheric CO2, Global Biogeochemical Cycles, **23**, GB1005, http://dx.doi.org/10.1029/2008GB003349.

Haine, T. W. M. and T. M. Hall, 2002: A generalized transport theory: water- mass composition and age, *J. Phys. Oceanogr.,* **32**, 1932-1946.

Haine, T.W.N, H. Zhang, D.W. Waugh, M. Holzer, 2008: On transit-time distributions in unsteady circulation models, *Ocean Modelling*, **21 (1)**, 35-45

Hall, T.M. and T.W.N. Haine, 2002: On ocean transport diagnostics: The idealized age tracer and the age spectrum, *J. Phys. Oceanogr*., **32 (6)**, 1987-1991

Halliwell, Jr., G. R., 2004: Evaluation of vertical coordinate and vertical mixing algorithms in the hybrid-coordinate ocean model (HYCOM), *Ocean Modelling*, **7**, 285-322.

Hartin, CA, Fine RA, Sloyan BM, Talley LD, Chereskin TK, Happell J. 2011: Formation rates of Subantarctic mode water and Antarctic intermediate water within the South Pacific. *Deep-Sea Research Part I-Oceanographic Research Papers*. **58**, 524-534.

Hartin, C., R.A. Fine, I. Kamenkovich, and B. Sloyan, 2014: Comparison of Subantarctic Mode Water and Antarctic Intermediate Water in the South Pacific between NCAR-CCSM4 and observations, *Geophys. Res. Lett.*, DOI: 10.1002/2013GL058728

Henning, C.C., and G. Vallis, 2005: The effects of mesoscale eddies on the stratification and transport of an ocean with a circumpolar channel. *J. Phys. Oceanogr*., **35**, 880-896.

Holzer, M. and T.M. Hall, 2002: Transit-time and tracer-age distributions in geophysical flows, *J. Atmos. Sci.*, **57**, 3539-3558.

Kamenkovich, I. and T. Radko, 2011: Role of the Southern Ocean in setting the Atlantic stratification and meridional overturning circulation. *J. Marine Res.,* **69**, 277-308

Khatiwala, S., M. Visbeck, and P. Schlosser, 2001: Age tracers in an ocean GCM, *Deep-Sea Res*., **48(6)**, 1423-1441.

Large, W.G., J.C. McWilliams, and S.C. Doney, 1994: Oceanic vertical mixing: A review and a model with a nonlocal boundary layer parameterization. *Rev. Geophys.*, **32***,* 363-403.

Maltrud, M., F. Bryan, and S. Peacock, 2010: Boundary impulse response functions in a century-long eddying global ocean simulation. *Environ Fluid Mech*., **10**, 275–295

617 Marshall, J., and T. Radko, 2003: Residual-mean solutions for the Antarctic Circumpolar Current
618 and its associated overturning circulation. *J. Phys. Oceanogr*., **33**, 2341-2354.

619 McCartney, M.S., 1982: Subantarctic Mode Water. A voyage of discovery. M. Angel, Ed. Deep-
620 Sea Res., 24 (Suppl.), 103-119.

621 McCartney, M.S., 1977: The subtropical recirculation of mode waters. J. Mar. Res., 40 (Suppl.),
622 427-464.

623 Peacock, S., and M. Maltrud, 2006: Transit-time distributions in a global ocean model, *J. Phys.*
624 *Oceanogr., 36*, 474-495.

625 Pennel, R., and I. Kamenkovich, 2014: On the factors controlling the eddy-induced transport in
626 the Antarctic Circumpolar Current. *J. Phys. Oceanogr.,* **44**, 2127-2138

627 Reid, J.L., 1965. Intermediate Waters of the Pacific Ocean. The Johns Hopkins Oceanographic
628 Studies 2, 85.

629 Sallee, J-B., R.J. Matear, S.R. Rintoul, A. Lenton, 2012: Localized subduction of anthropogenic car-
630 bon dioxide in the Southern Hemisphere oceans, *Nature Geoscience,* **5**, 579–584,
631 doi:10.1038/ngeo1523

632 Sloyan, B.M. and S.R. Rintoul, 2001: Circulation, renewal, and modification of Antarctic Mode
633 and Intermediate Water. *J. Phys. Oceanogr*., **31**, 1005-1030.

634 Sloyan, B. M., L.D. Talley, T.K. Chereskin, 2010: Antarctic Intermediate Water and Subantarc-
635 tic Mode Water Formation in the Southeast Pacific: The Role of Turbulent Mixing.
636 Source: J. Phys. Oceanogr., **40**, 1558-1574

637 Song, H., Marshall, J., Gaube, P., and McGuillicudy, D, 2015: Anomalous chlorofluorocarbon
638 uptake by mesoscale eddies in the Drake Passage region Journal of Geophysical Research,
639 vol. 120, no. 2, pp. 1065–1078, doi: 10.1002/2014JC010292

640 Sun, S., and R. Bleck, 2001: Thermohaline Circulation Studies with an isopycnic coordinate
641 ocean model, *J. Phys. Oceanogr*., **31**, 2761-2782.

642 Sun S., R. Bleck, C.G. Rooth, J. Dukowicz, E.P. Chassignet, and P. Killworth, 1999. Inclusion of
643 thermobaricity in isopycnic-coordinate ocean models. *J. Phys. Oceanogr.*, **29**, 2719-2729.

644 Talley, L.D., 1996: Antarctic Intermediate Water in the South Atlantic. The South Atlantic: Pre-
645 sent and Past Circulation, G. Wefer et al., Eds., *Springer*, 219-238.

646 Thiele and Sarmiento, 1990: Tracer Dating and Ocean Ventilation. *J. Geophys. Res.,* **95**, 9377-
647 9391

648 Tsuchiya, M., 1991: Flow path of the Antarctic Intermediate water in the western equatorial
649 South Pacific Ocean. *Deep-Sea Res.,* **38** (suppl.), S273-S279.

650 Wang, J., M. R. Mazloff, and S. T. Gille, 2014: Pathways of the Agulhas waters poleward of
651 29^{o}S, *J. Geophys. Res. Oceans*, **119**, 4234-4250, doi:10.1002/2014JC010049

652 Zalesak, S., 1979: Fully multidimensional flux-corrected transport algorithms for fluids. *J. Com-*
653 *putational Physics*, **31**, 335–362.

654

7 FIGURES

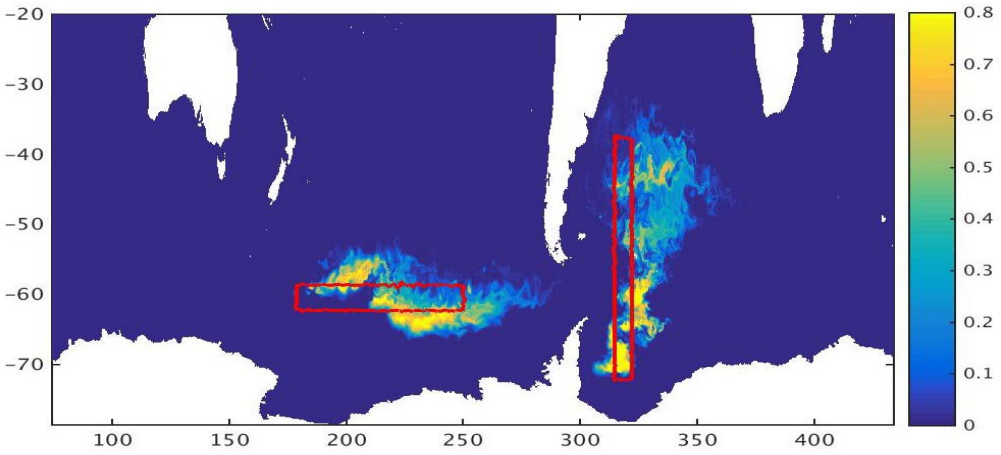

Figure 1: Evolution of the dye tracer; the initial (red lines) and concentrations at day 196 are shown in the top layer for the online case.

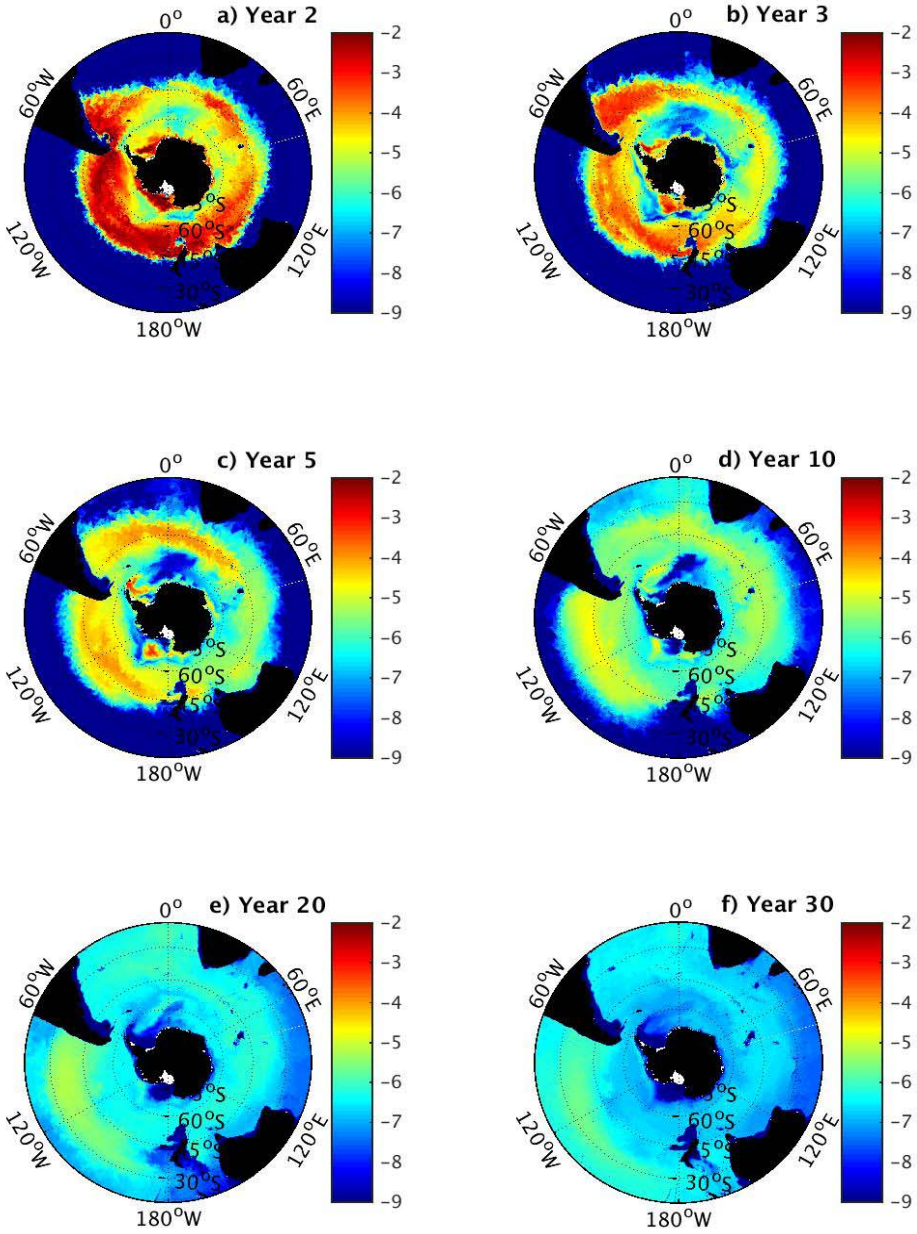

Figure 2: Horizontal spreading of the BIR tracer in the control (FULL_ADV) run. Logarithm of vertically integrated (over top model 25 layers) and divided by 5500 m. BIR concentrations are shown for different times (day 180 for each year). The depth of the 25th layer varies approximately between 1000 and 3500 m.

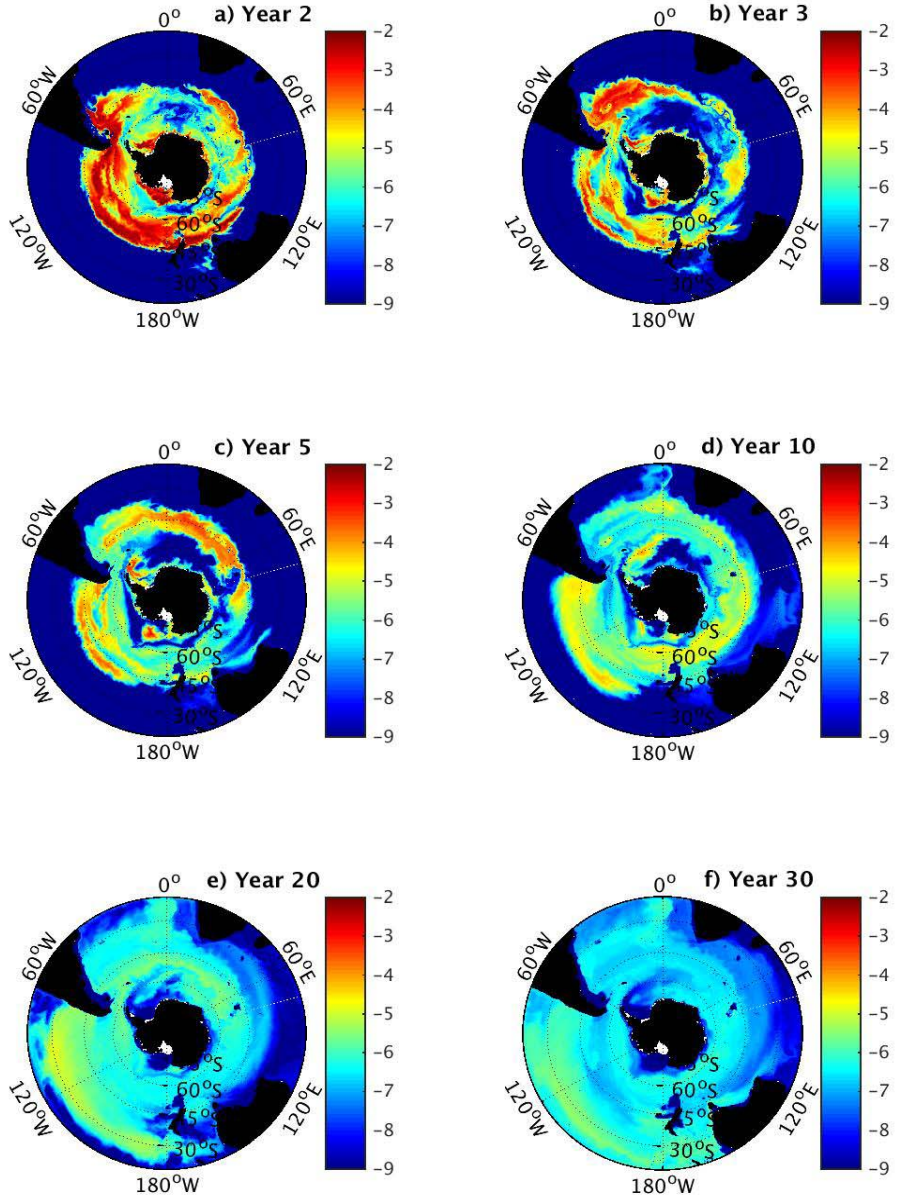

657

Figure 3: Horizontal spreading of the BIR tracer in the MEAN_ADV run. Logarithm of vertically integrated (over top model 25 layers) and divided by 5500 m BIR concentrations are shown for different times (day 180 for each year). The depth of the 25th layer varies approximately between 1000 and 3500 m.

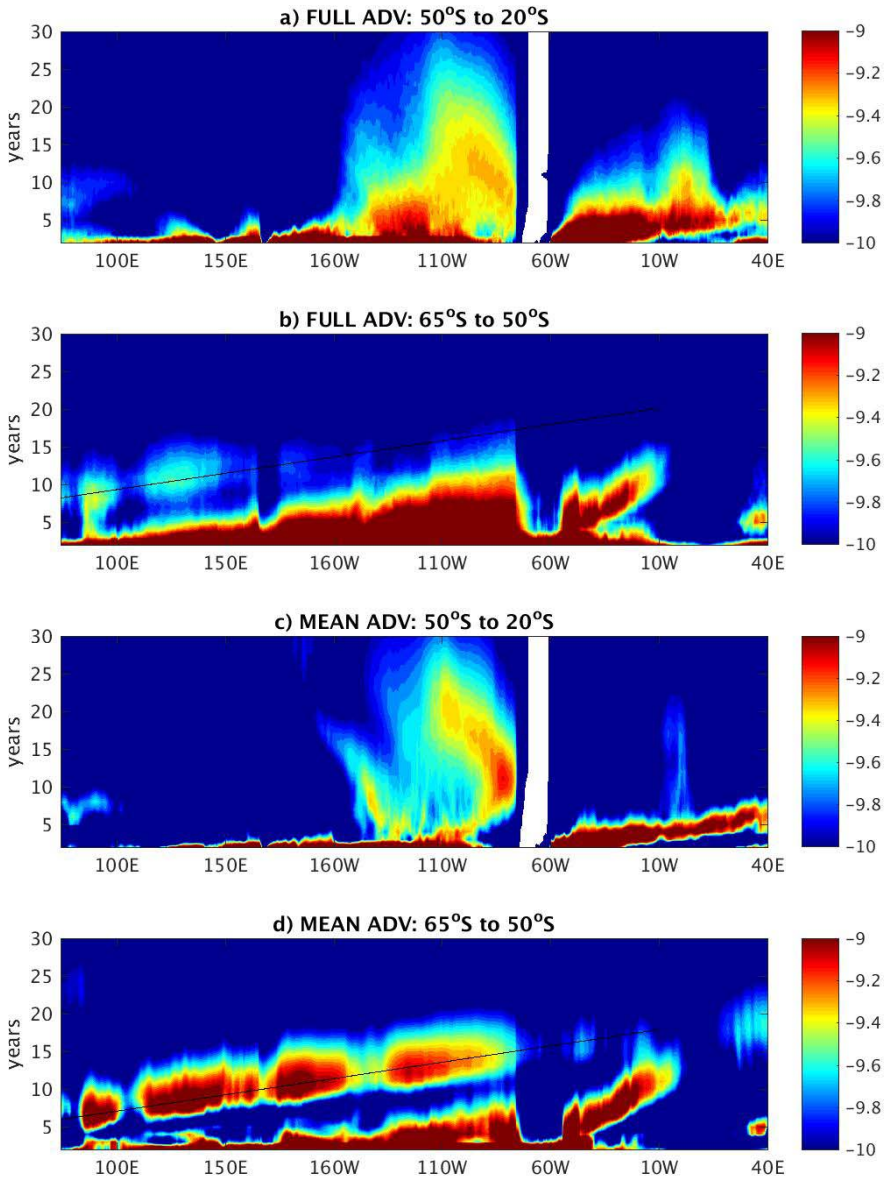

658

659 Figure 4: Hovmoller diagram of the zonal evolution of the BIR tracer. Logarithm of the meridio-
660 nally averaged and vertically integrated tracer values are shown as the function of longitude and
661 time in FULL_ADV (panels a and b) and MEAN_ADV (panels c and d) simulations Panels (a)
662 and (c) show values averaged within the 50°S to 20°S latitude range; panels (b) and (d) – 65°S to
663 50°S range; the black line illustrates propagation with a constant speed of 0.05 m sec^{-1}.

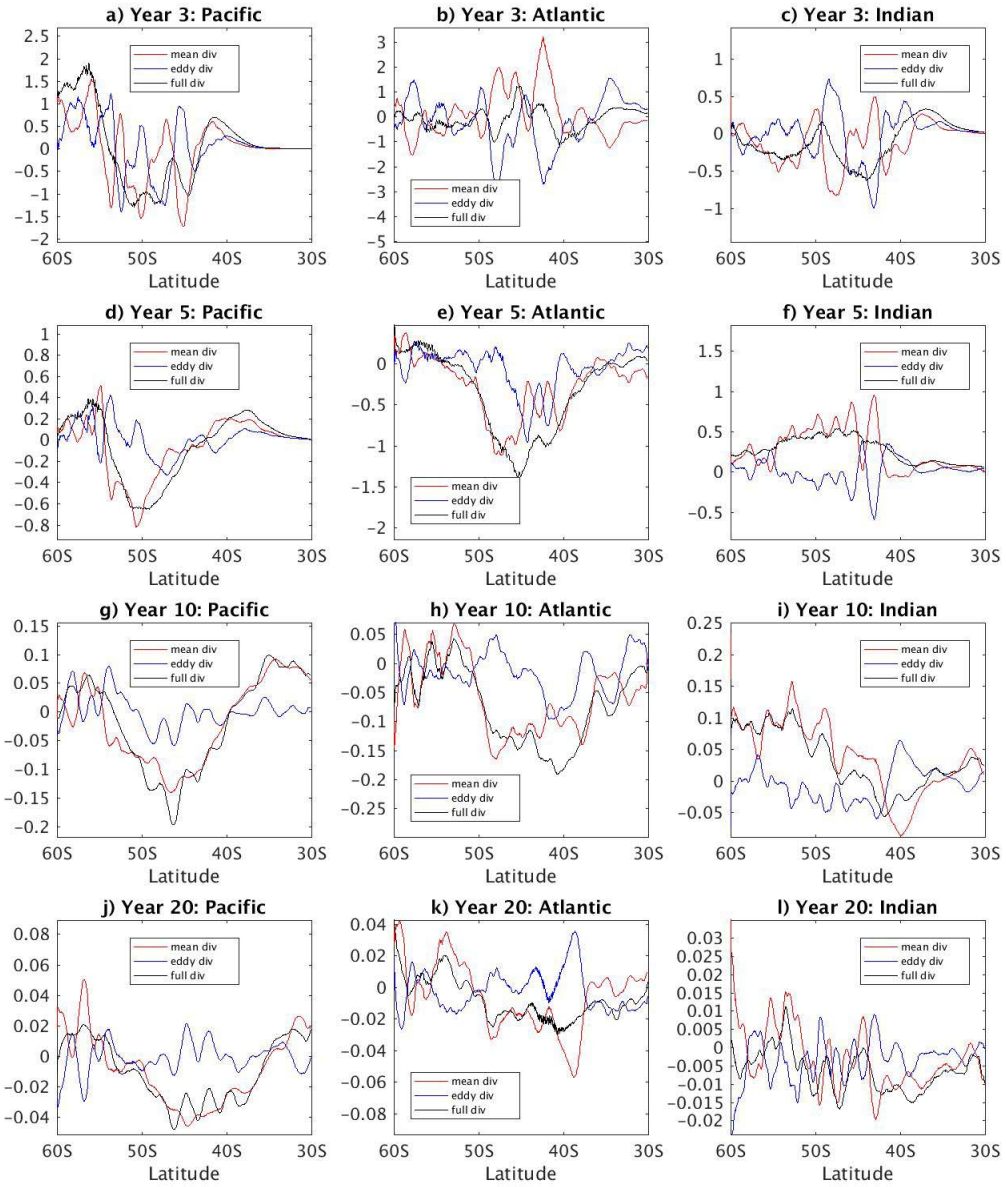

664

Figure 5: Divergence of BIR fluxes due to the mean currents ("mean advection" in Equation 3, red lines) and mesoscale eddy currents ("eddy advection" in Equation 3, blue lines), as well as their sum (black lines). Shown are the annual means of these terms for years 3 (first row), 5 (second row), 10 (third row) and 20 (fourth row). These terms are vertically integrated within the top 25 layers, zonal averaged within the Pacific (left column), Atlantic (middle column) and Indian (right column) sectors and smoothed for presentation purposes. Units are 10^{10}×m sec^{-1}.

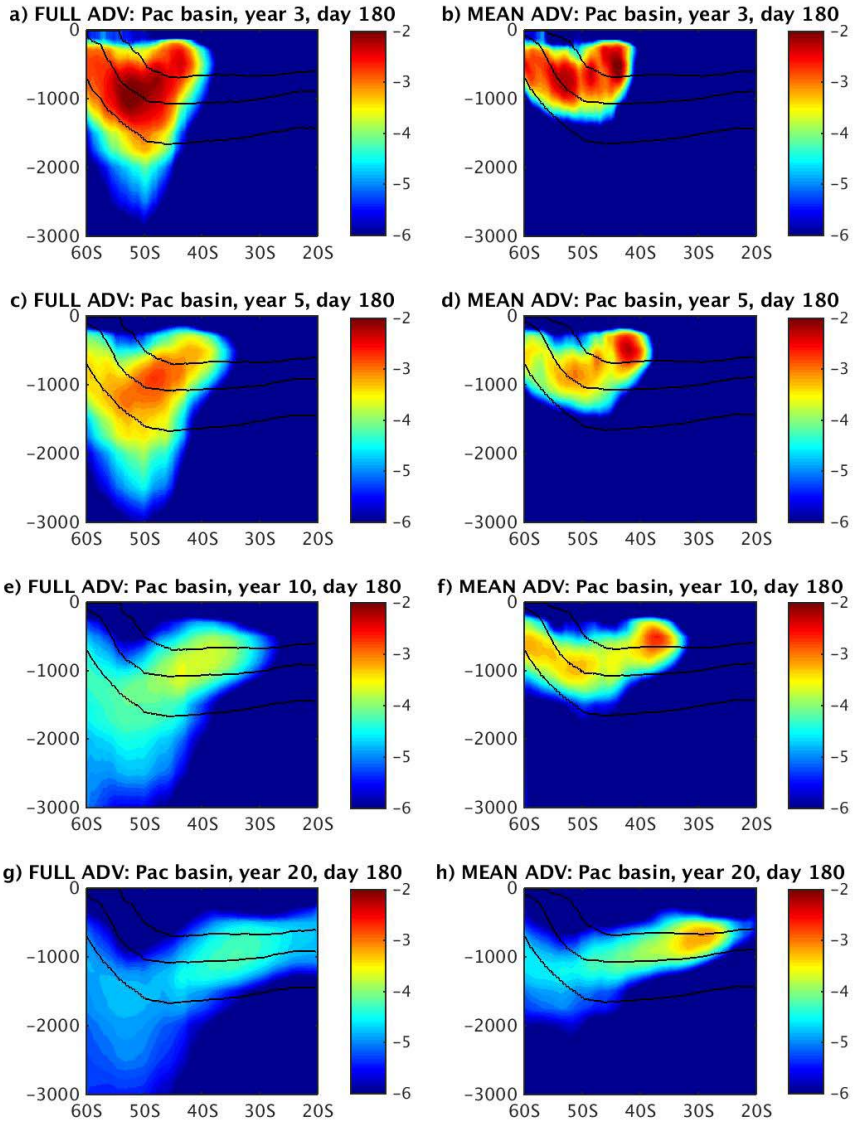

665

666 Figure 6 Ventilation of the Pacific sector. Logarithm of the zonally averaged BIR tracer is shown
667 north of 60°S and in the upper 2500 m in the control FULL_ADV (left column) and
668 MEAN_ADV (right column) cases. Black contours mark σ_θ isopycnals 26.8, 27.05 and 27.4 kg
669 m^{-3}.

670

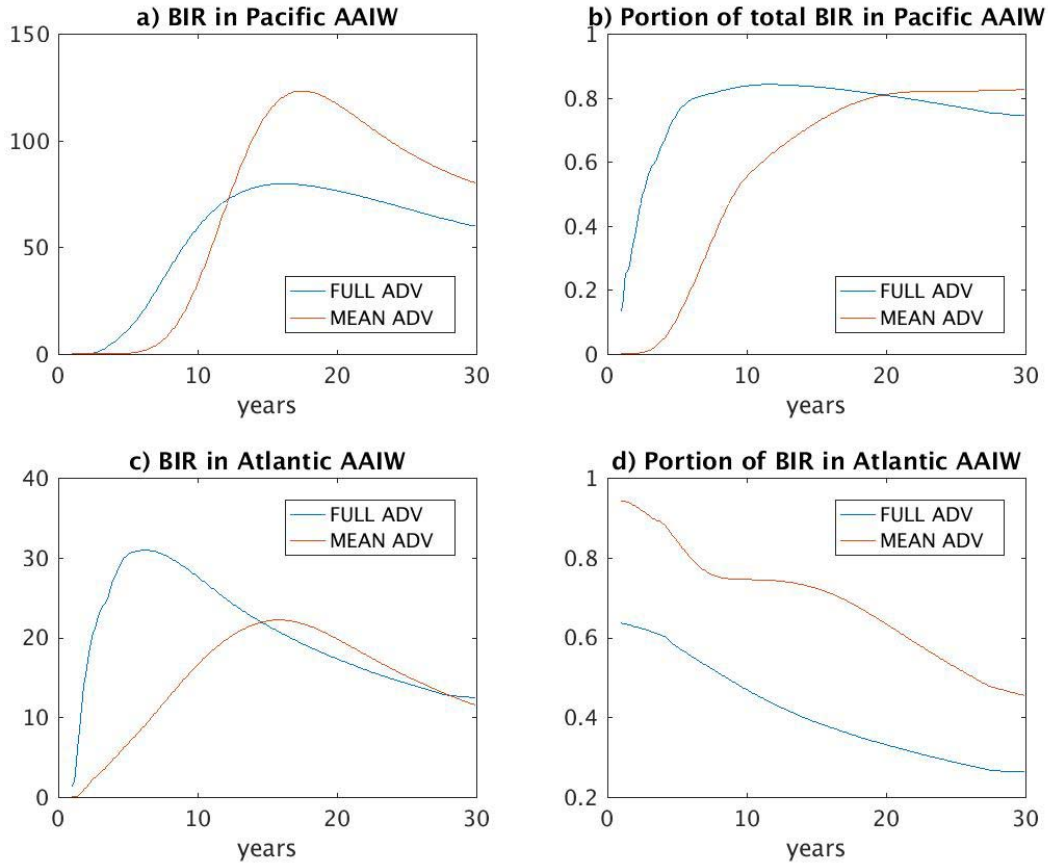

671

672 Figure 7: BIR inventory in the AAIW layer in the Pacific (top panels) and Atlantic (bottom
673 panels) sectors, as a function of time. BIR values are integrated for waters with either S= 34.2-
674 34.55 ppt or σ_θ =27.05-27.4 kg m^{-3}, and between 35°S and 30°S. (a,c) total integrated values (in
675 10^{12} m^3); (b,d) the same values divided by the total BIR inventory in the same geographical
676 regions. The results are smoothed in time for presentation purposes.

677

678

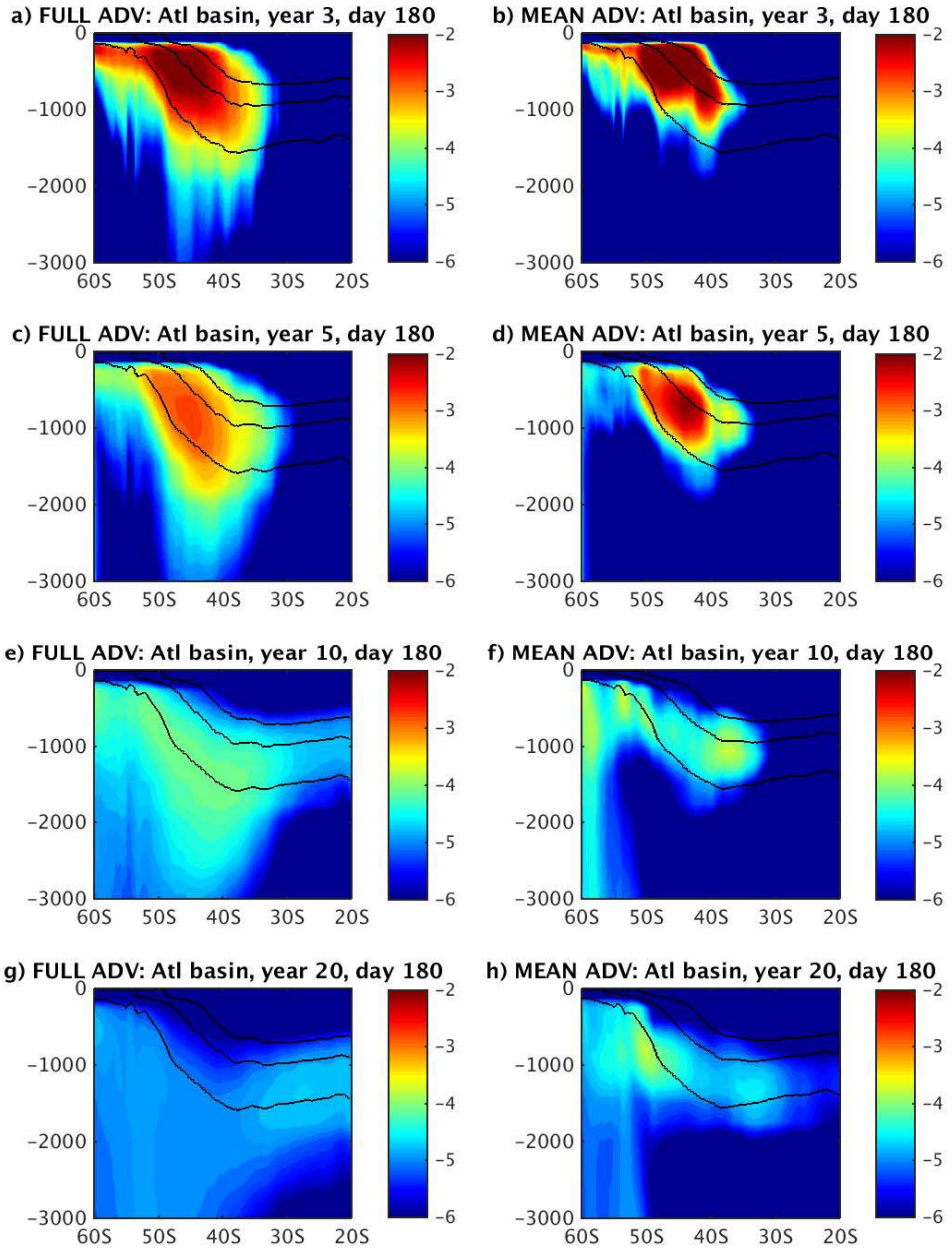

679

680 Figure 8: Ventilation of the Atlantic sectors. Logaritm of the zonally averaged BIR tracer is
681 shown north of 60°S and in the upper 2500 m in the control FULL_ADV (left column) and
682 MEAN_ADV (right column) cases. Black contours mark σ_θ isopycnals 26.8, 27.05 and 27.4 kg
683 m^{-3}.

684

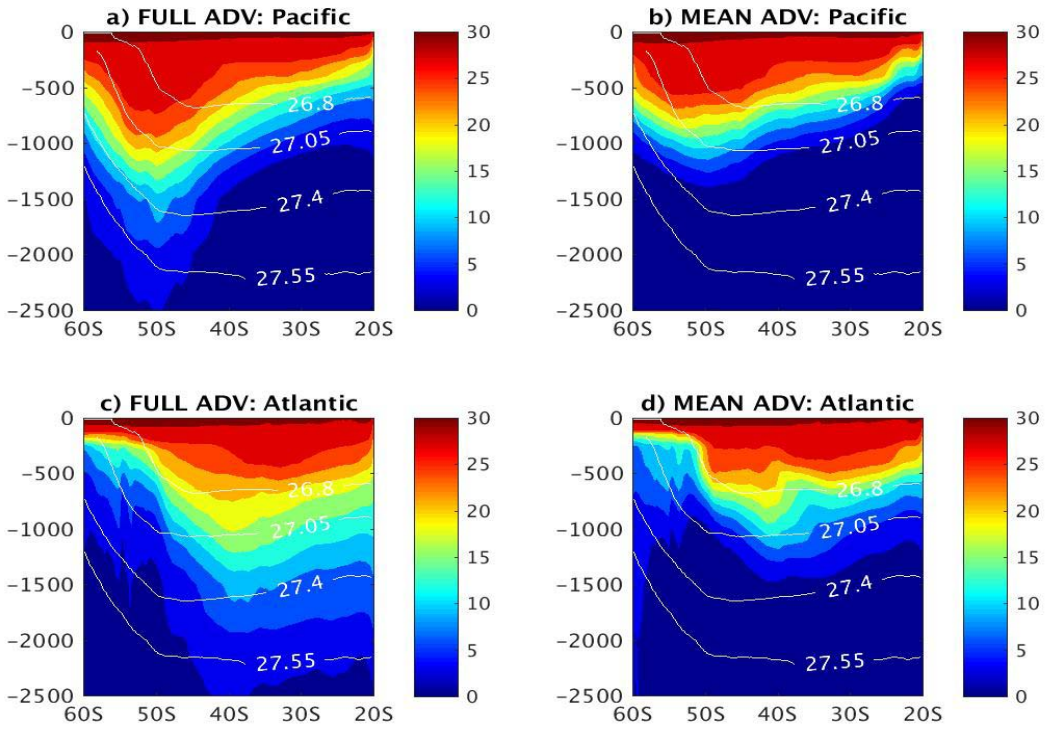

685

686 Figure 9: Zonally averaged TST tracer concentrations at year 30 is shown north of 60°S and in
687 the upper 2500 m for snapshots in the control FULL_ADV (left column) and MEAN_ADV
688 (right column) cases. Zonally averaged selected σ_θ isopycnals are shown in white.

689

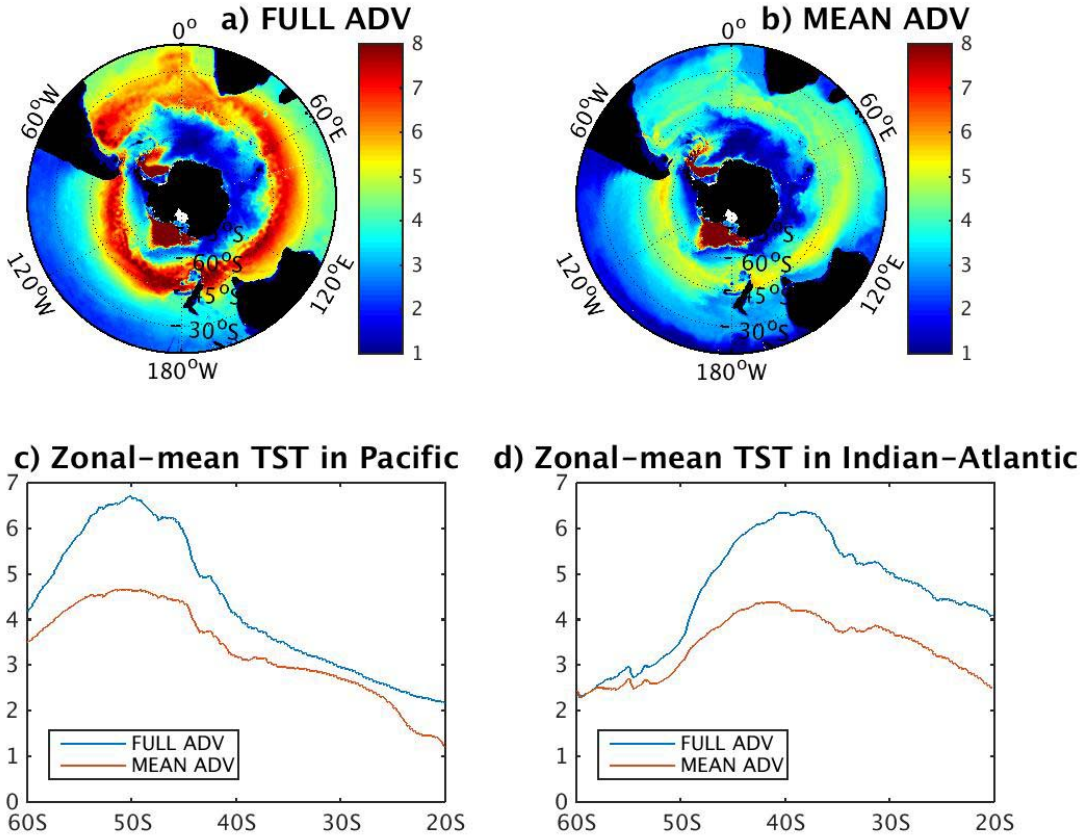

690

691

692 Figure 10: TST inventory (vertically integrated and divided by 5500m), in years, averaged over
693 the last 6 months of year 30: (a) FULL_ADV; (b) MEAN_ADV. Bottom row: same fields (in
694 years) but zonally averaged within: (c) the Pacific; and (d) the Atlantic-Indian basins.

695

696